Turbulence Measurements for a Longitudinal Vortex Interacting with a Three-Dimensional Turbulent Boundary Layer

Takaaki Shizawa* and John K. Eaton†
Stanford University, Stanford, California 94305

Turbulence measurements are reported for the case of a longitudinal vortex embedded in a pressure-driven, three-dimensional boundary layer. Previous measurements have shown that the distributed longitudinal vorticity of the three-dimensional boundary layer has a major effect on the mean flow development. The present measurements show that the turbulence development is very sensitive to the sign of the vortex. For one sign, the vortex-induced perturbation in the turbulence field decays quickly while for the opposite case the disturbance continues to grow producing high levels of turbulence kinetic energy and shear stress. This is caused by a strong velocity gradient in the outer part of the boundary layer. Generally, the structural parameter a_1 is suppressed below conventional boundary-layer levels.

Nomenclature

a_1 = structural parameter $-\overline{u'v'}/q^2$
q^2 = $\overline{u'u'} + \overline{v'v'} + \overline{w'w'}$
r = radius from vortex center
U = streamwise mean velocity component
V = wall-normal mean velocity component
W = spanwise mean velocity component
u',v',w' = fluctuating velocities
x = streamwise coordinate
y = wall-normal coordinate
z = spanwise coordinate
ν_T = eddy viscosity $-\overline{u'v'}/\partial U/\partial y$

Introduction

LONGITUDINAL vortices embedded in turbulent boundary layers are frequently used for flow control and also occur naturally in many situations. The interaction of embedded vortices with two-dimensional turbulent boundary layers has been the subject of intense research over the past 10 years. However, in most practical applications, embedded vortices interact with a three-dimensional boundary layer which lends further complexity to the problem.

A key feature of three-dimensional turbulent boundary layers (3DTBLs) is that they contain distributed longitudinal vorticity. For example, a simple pressure-driven 3DTBL has a sheet of concentrated longitudinal velocity near the wall, with a broader but less concentrated region of oppositely signed vorticity in the wake region. The rolled-up vorticity of the embedded longitudinal vortex may be expected to interact with the distributed vorticity of the boundary layer in a complex way leading to significant modifications in the vortex behavior. The exact nature of the interaction depends on the sign of the vortex circulation as will be seen below.

In a recent paper, Shizawa and Eaton[1] examined the interaction of an embedded longitudinal vortex with a pressure-driven three-dimensional (3D) boundary layer. The flow geometry is sketched in Fig. 1. The boundary layer of interest develops on the test wall in the plane of the page entering as a two-dimensional boundary layer at the left. The wedge splits and turns the flow creating a strongly skewed 3D boundary layer. A longitudinal vortex is generated just upstream of the 3D region, then interacts with the skewed boundary layer. Shizawa and Eaton showed that longitudinal vortices are attenuated very rapidly when embedded in a three-dimensional boundary layer. The peak vorticity level in the core of the vortex and the secondary velocities induced by the vortex decay over twice as fast as a similar vortex embedded in an otherwise two-dimensional (2D) boundary layer. Vortex-induced perturbations in the mean axial velocity also devel-

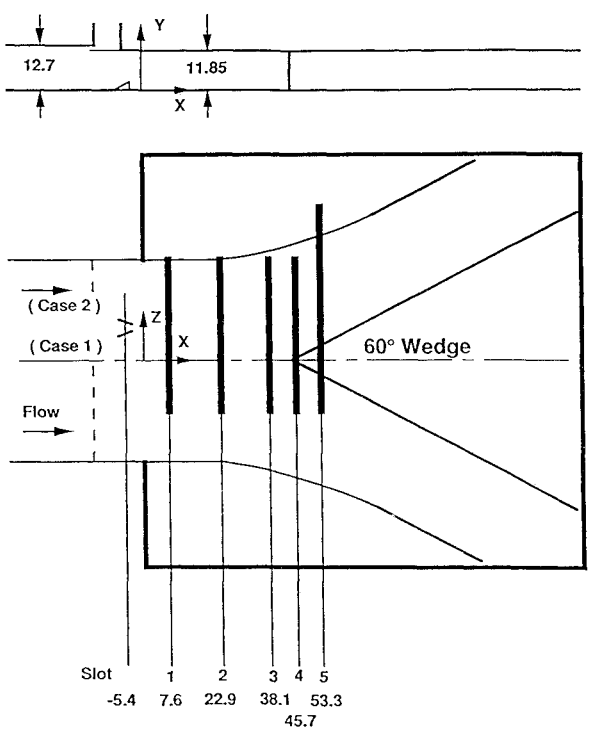

Fig. 1 Three-dimensional test section geometry. Dimensions in centimeters.

Presented as Paper 91-0732 at the AIAA 29th Aerospace Sciences Meeting, Reno, NV, Jan. 7-10, 1991; received Sept. 13, 1990; revision received March 2, 1991; accepted for publication March 5, 1991.

*Research Associate, Department of Mechanical Engineering; currently at Science Univeristy of Tokyo, 1-3 Kagarazaka, Shinjuku-ku, Tokyo, 162, Japan.

†Professor, Department of Mechanical Engineering. Member AIAA.

oped differently than in a 2D boundary layer with the development depending strongly on the vortex sign.

These results have significant implications for separation control applications of longitudinal vortices. It has been assumed that separation delay is caused by transport of high momentum fluid toward the wall by the mean vertical velocity of the vortex. However, modern work (cf. Westphal et al.[2]) has shown that an embedded vortex diffuses very rapidly so the secondary velocities in the boundary layer die out quickly. Separation delay is instead caused by the reduction in average boundary-layer thickness that develops before the vortex diffuses (see Arnaud and Russell[3]) and by the high turbulence levels associated with the vortex-induced perturbation of the axial velocity field. It is thus important to understand how the turbulance development is affected by overall boundary-layer three-dimensionality.

The mean flow results also have implications for flow modeling. The strong differences between vortex development in 2D and 3D boundary layers are attributed to differences in the flow around the crossflow separation line. The details of this separation zone are probably sensitive to both the cross-flow velocity profile in the 3DTBL and the secondary velocity field in the vortex. Thus, the velocity field must be accurately predicted in the cross-flow plane in order to get even a qualitatively correct prediction of the overall flow development. Details of the turbulance stress field in the vicinity of the vortex–boundary-layer interaction must be understood if such a prediction is to be made.

The objectives of the present study were then to provide measurements of the turbulent stress field for both of the cases described above. Of particular interest were any significant differences between the cases in terms of overall turbulence kinetic energy levels. The data were also evaluated in terms of simple turbulence models, although no complete calculations of the flow were attempted.

There have been several recent studies examining the details of vortex–boundary-layer interactions motivated by the desire to extend existing computational techniques to complex three-dimensional flows. Extensive reviews of these studies and other research on vortex–boundary-layer interaction are contained in Pauley and Eaton[4] and Shizawa and Eaton.[5] Bradshaw and co-workers (Shabaka et al.,[6] Mehta and Bradshaw[7]) provided the first detailed turbulence data for vortex–boundary-layer interactions finding the Reynolds shear stress field to be highly distorted with both the shear correlation coefficient and the stress/energy ratio drastically different than in a two-dimensional boundary layer. They concluded that full Reynolds-stress modeling is required to predict such a flow. Later studies by Takagi and Sato,[8] Eibeck and Eaton,[9] Westphal et al.,[2] Matsumoto,[10] and Pauley and Eaton[4] provided more detailed data for a variety of configurations. An important feature in many of the studies was a velocity deficit in the vicinity of the core. This deficit is characteristic of vortices generated by wall-mounted vortex generators. Associated with the deficit are large regions of negative shear stress (positive $\overline{u'v'}$) and large values of the turbulent kinetic energy. The region of negative shear stress does not correspond precisely to the region of reversed velocity gradient so the eddy viscosity is negative in the vicinity of the vortex. A second important feature is the tongue of highly turbulent fluid which lifts away from the wall on the upwash side of the vortex and diffuses into the surrounding flow. This was especially obvious in the study of Cutler and Bradshaw,[11] who examined the interaction of the boundary layer with a strong vortex pair moving down toward the wall from a delta wing.

Experimental Methods

The experiments were conducted in the open-circuit, boundary-layer wind tunnel used by Anderson and Eaton[12] and Pauley and Eaton.[4] The measurement techniques and wind-tunnel control hardware were nearly identical to those used previously so they are described only briefly here. The wind tunnel was specially developed to investigate three-dimensional boundary layers. The boundary layer of interest developed as a two-dimensional layer in a 61 × 12.7 cm rectangular duct before entering the three-dimensional test section. At this point the boundary layer was 3.1 cm thick with a momentum thickness Reynolds number of 3700 at a freestream velocity of 16.5 m/s. Within the test section, the boundary layer was split in two and turned by a symmetrical 60-degree wedge as illustrated in Fig. 1. The embedded vortex was introduced just upstream of the three-dimensional section using a 2-cm-high, half-delta-wing vortex generator at an 18-degree angle of attack. The generator was positioned so the vortices for the two different cases passed through the same point midway through the 3D test section.

Three-component mean velocity measurements were acquired using the five-hole pressure probe described by Pauley and Eaton.[4] The correction scheme described by Westphal et al.[2] was used to correct for the effects of velocity gradient across the probe. The uncertainty in the corrected measurements was estimated to be 1.5% for the velocity magnitude and 0.5 degree for the flow angle.

A rotatable cross-wire probe was used to acquire five of the six Reynolds stress components and 7 of the 10 triple products. The unmeasured Reynolds component was the secondary shear stress, $\overline{v'w'}$. The techniques used were basically the same as those described by Anderson and Eaton.[12] The analysis procedure neglected the out-of-plane velocity component. To minimize the effect of this assumption, the probe was aligned with the mean flow direction at every measurement position. The probe was automatically calibrated in the tunnel freestream and recalibrated after each profile. The data were rejected if the calibrations varied by more than 1%. Anderson and Eaton estimated the uncertainty in the measurements to be 5% for the normal stresses and 10% of $\overline{u'v'}$ for the shear stress components.

The coordinate system used for the measurements is shown in Fig. 1. Data were acquired on the five planes labeled 1 through 5 on Fig. 1. The probes were inserted through slots in the wall opposite the test wall. The slots were sealed by foam tape when a probe was in place and by a flush-fitting plug at other times. Probes were traversed by a two-axis computer-controlled traverse gear. The probe calibration, traversing, data acquisition, and data analysis procedures were performed on a Masscomp laboratory computer system.

Results and Discussion

Two different cases were examined using the identical baseline flow and vortex generator and changing only the sign of the generator angle of attack and the spanwise position of the generator. For case 1, the generator angle was set to produce a counter-clockwise vortex rotation looking upstream. The generator was positioned at $x = -5.4$ cm and $z = 8.0$ cm for this case. The vortex sign was opposite for case 2 with the generator positioned at $x = -5.4$ cm and $z = 11.5$ cm. The image vortex below the wall causes the vortex to move in the positive Z direction for case 1 and in the negative Z direction for case 2. With the present vortex generator positions the vortex center position for the two cases coincided at measurement slot 3. Data were obtained for both cases at five streamwise stations ($x = 7.6$, 22.9, 38.1, 45.7, and 53.3 cm). The data within the planes were acquired on a uniform grid with ½ cm spacing with the points closest to the wall being $y = ¼$ cm.

The complete three-component mean velocity data were presented in previous papers. To orient the reader and facilitate the discussion, the axial velocity field is presented here in Figs. 2 and 3. Each of the figures shows five contour plots acquired from the five measurement slots. The bottom plot in each figure is from the first measurement slot and the top

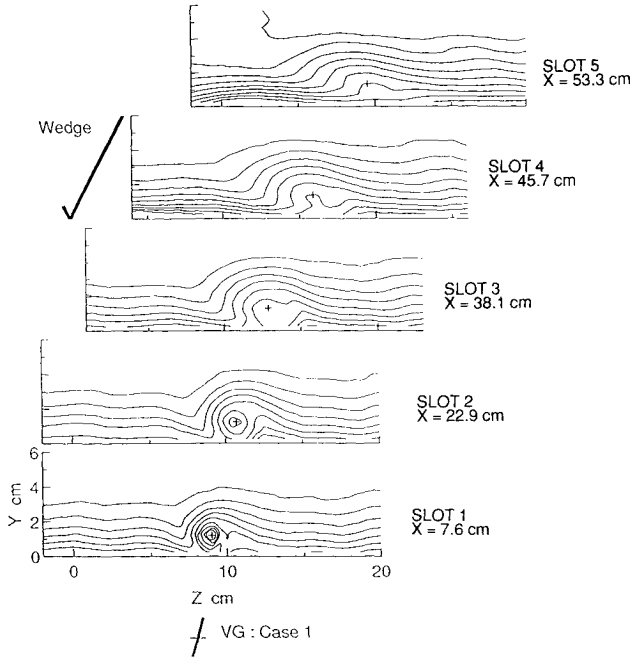

Fig. 2 Axial mean velocity for case 1. Outer contour level U/U_e = 0.99. Contour interval U/U_e = 0.05.

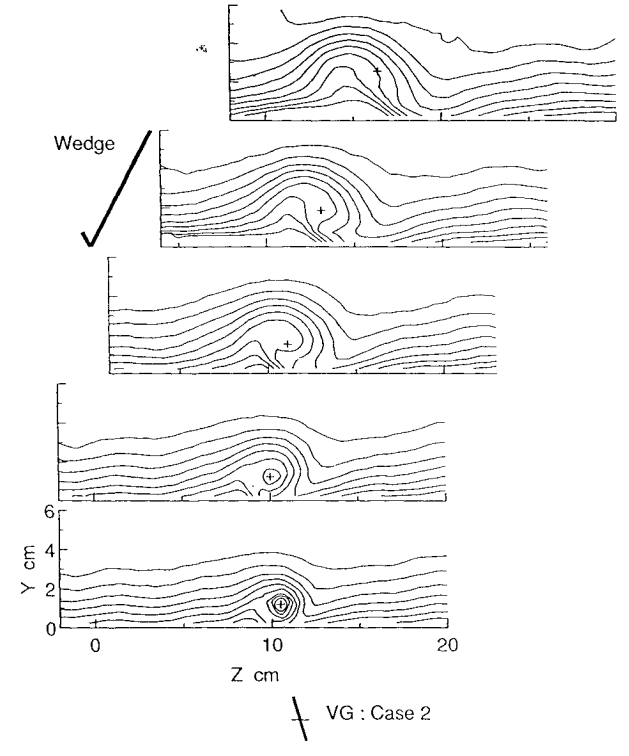

Fig. 3 Axial mean velocity for case 2.

plot is from the last. The vortex is swept to the side by the flow turning so the center of the measurement area is shifted to larger Z at downstream stations. The plots are aligned so that a vertical line drawn across the figure is a line of constant Z for all five plots.

There are strong differences in mean velocity development between the two cases. When the vortex sign is the same as the outer layer 3DTBL vorticity (labeled case 1), crossflow separation on the upwash side of the vortex is suppressed. The vortex-induced perturbation in the axial velocity field dies out very rapidly as shown in Fig. 2. With the opposite vortex sign (labeled case 2), the 3DTBL crossflow opposes the vortex-induced crossflow near the wall and there is a strong crossflow separation. This creates a tongue of low momentum fluid extending from the crossflow separation line to the outer part of the boundary layer as shown in Fig. 3. The perturbation in the axial velocity field continues to grow through the final measurement station.

The turbulence data are all presented as contour plots in the same fashion as the mean velocity data. In each plot the edge of the boundary layer (δ_{99}) is indicated by a dashed line and the location of peak vorticity is indicated by a + sign. The three normal stresses all develop in a similar fashion so we present here only plots of the sum of the normal stresses, that is, twice the turbulent kinetic energy. The kinetic energy development is shown in Figs. 4 and 5. At the first station the plots are dominated by the highly turbulent wake of the vortex generator. The wake and the associated turbulence decay rapidly and there is no evidence of a central peak beyond the second station. By the third station, the differences between the cases become quite apparent. In case 1, there are minor distortions in the contours which decay slowly toward a two-dimensional distribution. In case 2, both the overall distortion of the contours and the peak kinetic energy levels in the field continue to increase through the final measurement station. Two regions of high-turbulence kinetic energy develop in case 2. A peak develops above the vortex and is apparently still growing by the final measurement station. A second peak develops near the wall to the left of the vortex core. This latter peak is probably caused by advection of turbulence away from the wall in the vicinity of the crossflow separation line.

The primary shear stress component ($-\overline{u'v'}$) is shown in Figs. 6 and 7. Negative shear stress values (positive $\overline{u'v'}$) are shown as dotted contours. The case 1 vortex shows the typical distortion found when a vortex interacts with a 2D layer. The region of negative shear stress corresponds to a reversal of the velocity gradient, which is apparent in Fig. 2. It is surprising to see the persistence of this negative shear stress to

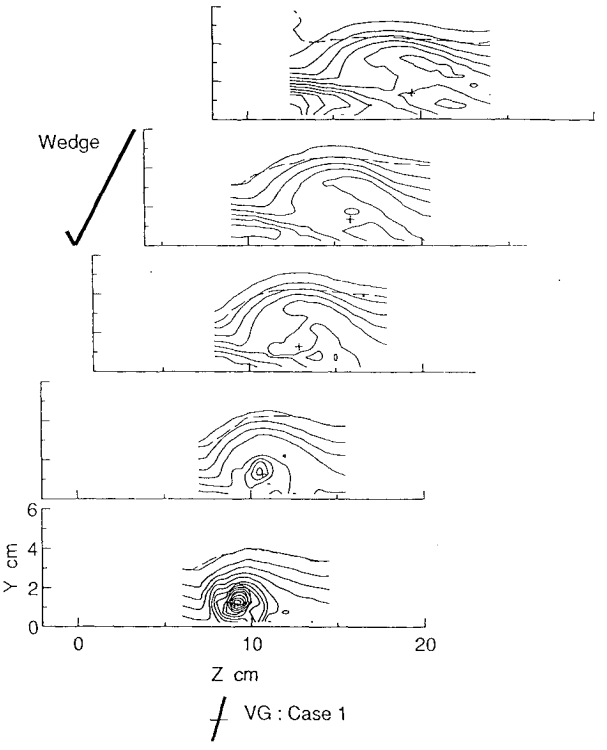

Fig. 4 Turbulence kinetic energy for case 1. Outer contour level q^2/U_e^2 = 0.001. Contour interval = 0.002.

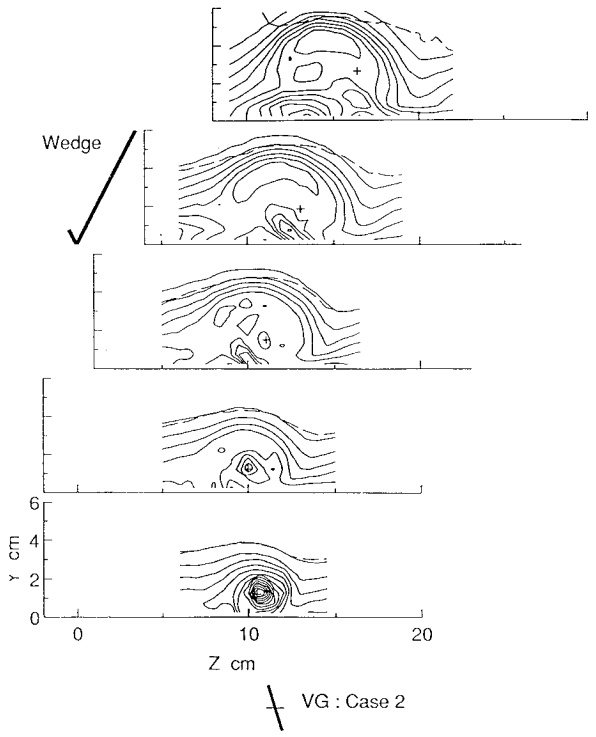

Fig. 5 Turbulence kinetic energy for case 2.

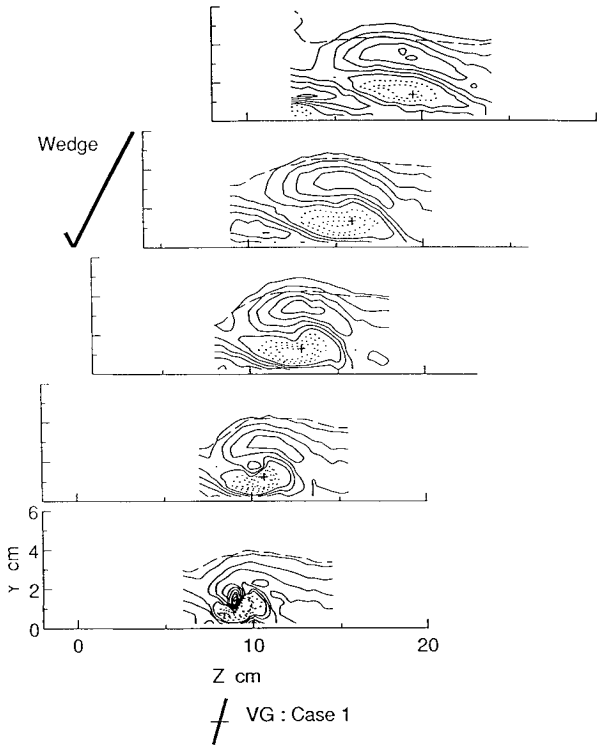

Fig. 6 Primary shear stress for case 1. Outer contour level $-\overline{u'v'}/U_e^2 = 0.0002$. Contour interval = 0.0003. Negative values shown dotted.

the end of the three-dimensional test section. By the final station, there are no significant regions of reversed velocity gradient. A similar region of negative shear stress is also seen in case 2. The more striking feature of case 2, though, is the region of strong positive shear stress which develops well away from the wall. This may be due both to advected turbulence as well as the strong velocity gradient in the outer layer for

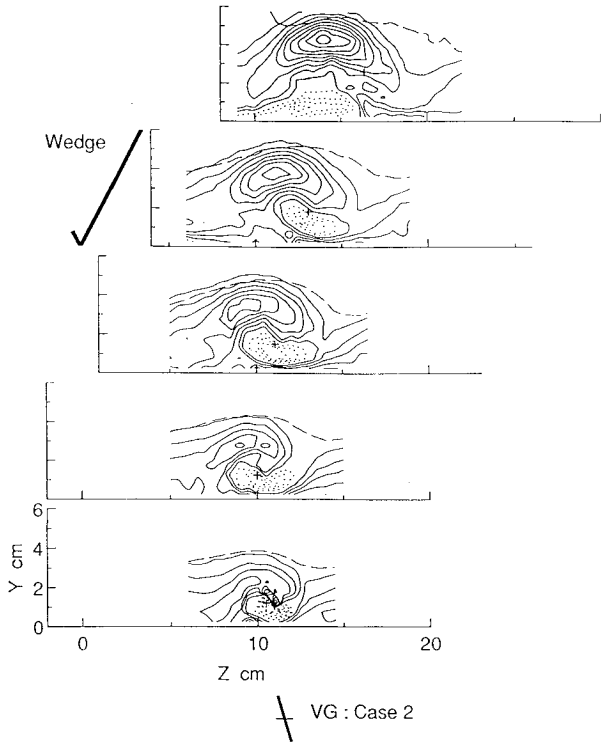

Fig. 7 Primary shear stress for case 2.

this case. Previous studies have found that the embedded vortex causes reductions in the structure parameter a_1 below the typical boundary layer value of 0.16. The same result was found in the present study as shown in Figs. 8 and 9. In these figures, dotted contours represent a_1 levels less than 0.12, so broad regions of dotted contours generally indicate a region of strongly suppressed structural parameter. For case 1, a_1 is lower than normal for nearly the entire field. It should be noted that a_1 is also suppressed by the introduction of three-dimensionality in the absence of the vortex (cf. Anderson and Eaton[12]). In case 2, the structure parameter is again reduced over most of the field except for a region at the top of the upwash tongue where nearly normal values are achieved. This suggests that the high turbulence levels in this region are produced locally by the strong velocity gradient.

The effects of stabilizing rotation or streamline curvature must be considered in examining the reduction in shear stress and particularly the precipitous drop of a_1. It should be noted first that curvature effects are unimportant in the baseline three-dimensional flow since the curvature is entirely in planes parallel to the wall. Reductions of a_1 in the baseline flow are most likely caused by rotation of dominant eddies out of their preferred orientation by the mean longitudinal vorticity (Bradshaw and Pontikos[13]). However, rotation effects are probably very important in suppressing turbulence near the vortex core. To estimate the importance of this effect we attempted to evaluate the gradient Richardson number, which Bradshaw[14] approximated for a slender axisymmetric flow as

$$\frac{2\dfrac{V_\theta}{r^2}\dfrac{\partial}{\partial r}(V_\theta r)}{\left(\dfrac{\partial U}{\partial r}\right)^2 + \left(\dfrac{\partial V_\theta}{\partial r}\right)^2}$$

Typically, curvature effects become significant for Ri greater than about 0.01 with complete stabilization of turbulence above $Ri = 0.25$. The Richardson number can be evaluated directly from the data at the first two measurement stations where the secondary velocities are large. Examining first the vortex

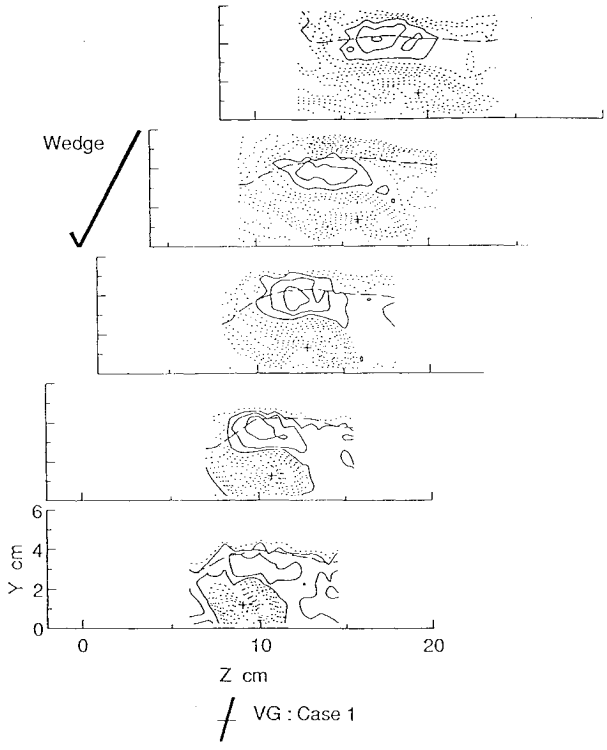

Fig. 8 Structural parameter a_1 for case 1. Solid contour levels start from 0.12 and increase in intervals of 0.02. Dotted contours start at 0.10 and decrease in intervals of 0.02.

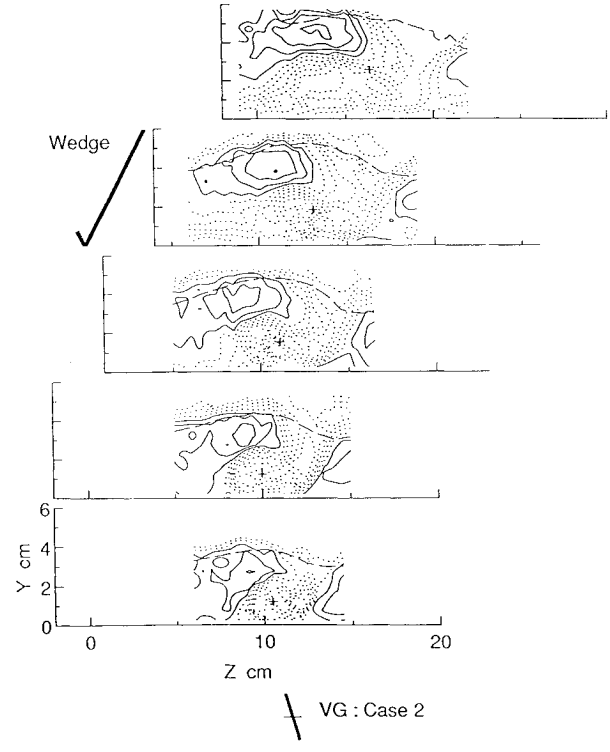

Fig. 9 Structural parameter a_1 for case 2.

core region, we find that Ri is of the order of 1 at the first measurement station decreasing rapidly downstream. Strong suppression of the turbulence is expected and indeed a_1 is found to be very small throughout the core region. However, high values of the turbulent kinetic energy are present in the generator wake at the first measurement stations. In other regions of the flow, rotation effects are apparently negligible. For example, in the region of high shear stress and kinetic energy above the vortex, the turbulent stresses remain large and indeed grow in case 2. Also, the value of a_1 is typical of uncurved shear layers.

There appears to be little hope that simple turbulence models can be applied successfully to this flow. Figs. 10 and 11 show contour plots of the eddy viscosity. Large values of the eddy viscosity have been suppressed in the contour plots because the velocity gradient passes through zero at several points in

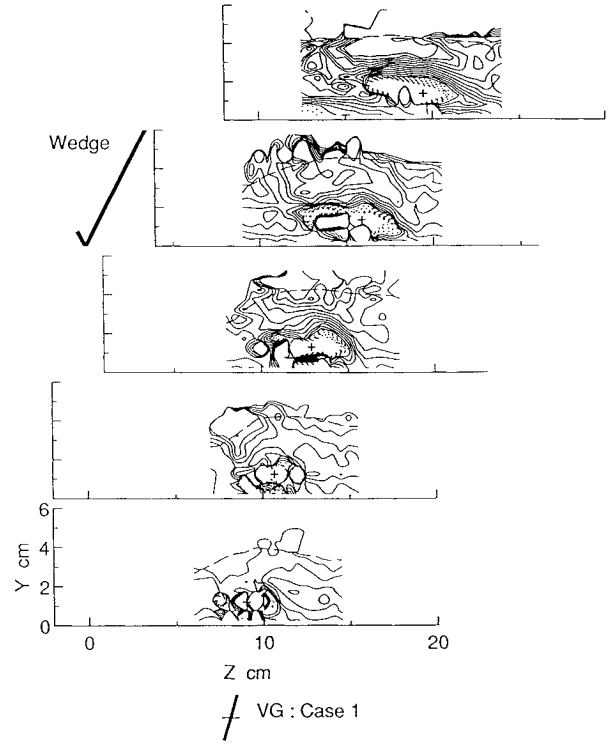

Fig. 10 Eddy viscosity $\nu_T/\delta U_e$. Outer contour level = 0.0002. Contour interval = 0.0004. Negative contours shown dotted.

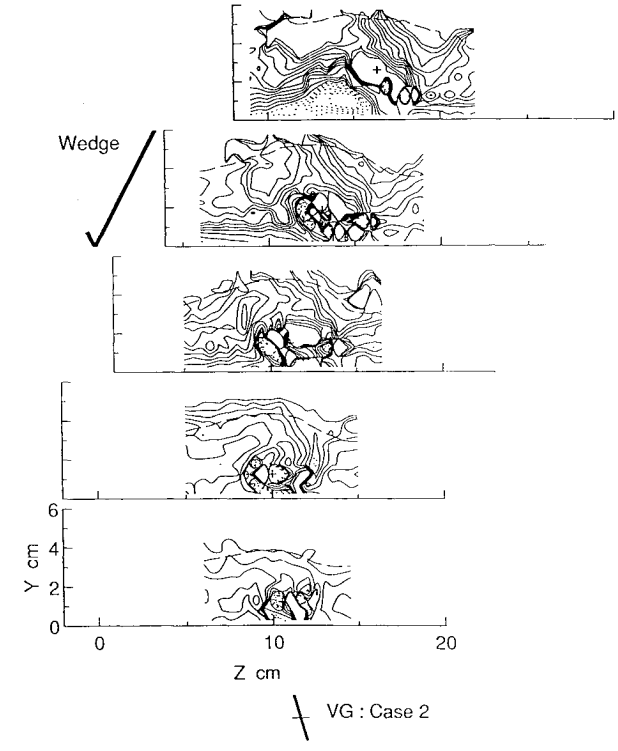

Fig. 11 Eddy viscosity for case 2.

each plane. Even ignoring this problem, the eddy viscosity plots are extremely complicated. At the first two stations, the eddy viscosity is reasonably uniform near the edge of the field. This section of the boundary layer appears much like an ordinary 2D boundary layer. However, the plots become increasingly complex going downstream, especially in case 2. Solution of the full stress-transport equations is probably required to accurately predict the stress distribution of this flow. In that case it is important to determine which terms of the equations are most important to calculate or model correctly. Initially, one might expect that advection of the stresses by the secondary flow would dominate, meaning that the secondary flow velocity would have to be calculated very accurately. However, the data suggest that production and dissipation dominate the evolution of the Reynolds stresses. Regions of high-turbulence kinetic energy and shear stress are generally associated with high mean velocity gradient away from the wall. To assess the relative importance of these terms correctly, the production and advection terms of the stress transport equations for the turbulent kinetic energy and the primary shear stress were evaluated directly from the data. For brevity, the results are presented here only for the primary shear stress ($-\overline{u'v'}$) and only for case 2. The remaining results are available in Ref. 5.

The production and advection terms for the primary shear stress are shown in Figs. 12 and 13. Gains are shown as solid contours and losses are dotted. It should be noted that one term in the production, $\overline{v'w'}\partial U/\partial z$ was not measured. This term was expected to be small for much of the field since Pauley and Eaton found that $\overline{v'w'}$ was typically at least four times smaller than $\overline{u'v'}$. The dominant term in the production is $\overline{v'^2}\partial U/\partial y$. The most important feature in the shear stress plots (Fig. 7) is the large peak which develops above the vortex. Figs. 12 and 13 shows that the peak is caused by high levels of production as opposed to significant advection from the wall region. Production of negative shear stress accounts for the development of a broad region of negative shear stress. The secondary velocities are somewhat larger in this region

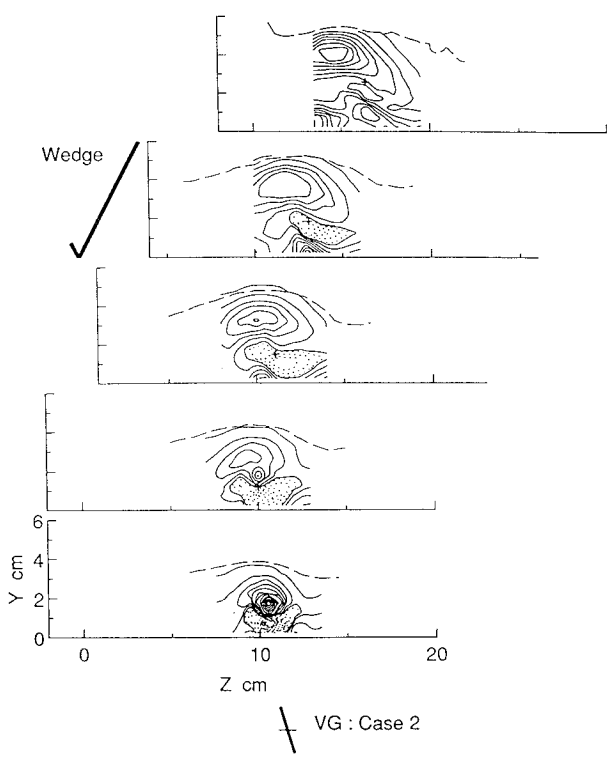

Fig. 12 Production of shear stress for case 2. Normalized by U_e^3/δ. Outer contour level = 0.0001. Contour interval = 0.0005. Negative contours shown dotted.

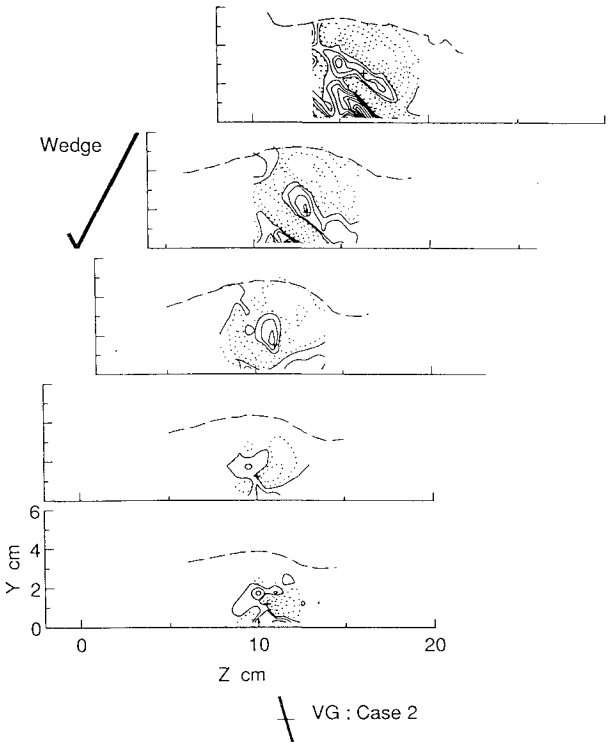

Fig. 13 Advection of shear stress for case 2. Contour levels as in Fig. 12.

and the advection does act to move the negative shear stress region to the left relative to the vortex core.

With the large peak in shear stress located well away from the wall, we might expect turbulent diffusion of shear stress to become important. The turbulent diffusion term for primary shear stress is:

$$\frac{\partial \overline{u'^2v'}}{\partial x} + \frac{\partial \overline{u'v'^2}}{\partial y} + \frac{\partial \overline{u'v'w'}}{\partial z}$$

We measured only the term $\partial\overline{u'^2v'}/\partial y$, which is probably the dominant term. This term is plotted in Fig. 14. Again losses are indicated as dotted contours. Clearly turbulent diffusion is minor except above the vortex where it acts to spread the shear stress peak.

Summary and Conclusion

This research has shown that the development of a boundary layer with an embedded longitudinal vortex is very sensitive to crossflow in the boundary layer and the sign of the vortex relative to the crossflow. If the crossflow direction is opposite the vortex-induced flow near the wall (case 2), then a strong crossflow separation results. In the opposite case (case 1), crossflow separation is suppressed and vortex-induced perturbations in the boundary layer decay quickly.

The turbulence development for case 1 is in line with the mean flow development. There are initially high levels of turbulence kinetic energy in the vortex generator wake which decay quickly. The remaining perturbations in the kinetic energy distribution die out rapidly, approaching a two-dimensional distribution even in the short length of the present test section. The shear stress distribution is considerably more complex, including a significant region of negative shear stress and a minor peak above the vortex. Once again though, the overall perturbation becomes relatively minor by the end of the test section. The turbulence field is drastically different in case 2, where the strong crossflow separation produces strong velocity gradients in the outer part of the boundary

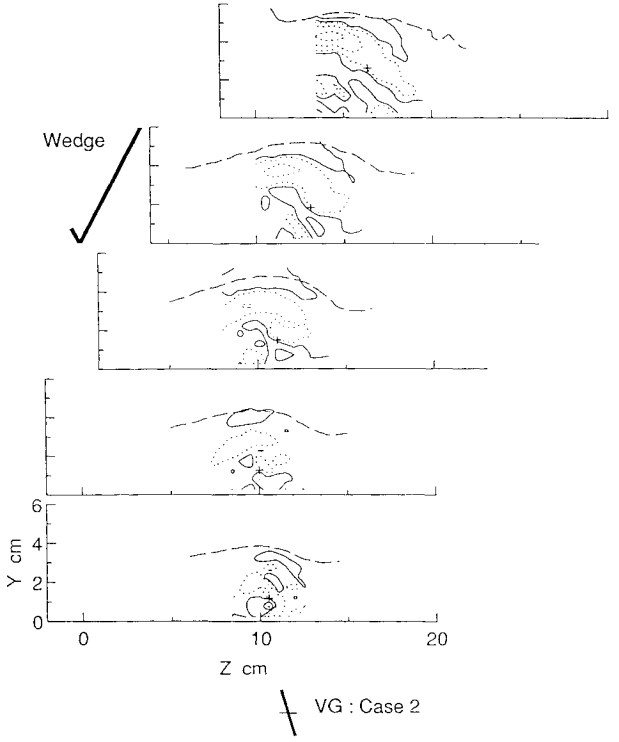

Fig. 14 Diffusion of shear stress for case 2. Contour levels as in Fig. 12.

layer. This leads to a substantial outer layer peak in both the kinetic energy and shear stress. It would thus be expected that a case 2 vortex would be far more effective in separation control applications.

Conventional turbulence models will probably not work well at predicting the Reynolds stress field. The stress/energy ratio a_1 was far below typical levels for both cases. Also, the eddy viscosity distributions were exceedingly complicated. However, the inaccuracies of the models may not prevent adequate prediction of the overall flow development. Much of the complexity in the eddy viscosity field is due to the existence of regions of very low velocity gradient. Inaccurate prediction of the relatively low shear stress in these regions may not have significant impact on the computation of the mean velocity field. The sensitivity of the vortex development to the crossflow suggests that computational methods will have to predict accurately the crossflow velocity profile of the three-dimensional boundary layer. Computational studies are needed to determine if the complexities of the turbulence field will strongly affect the overall accuracy of flowfield predictions.

Acknowledgments

We gratefully acknowledge financial support from the U.S. Department of Energy, Basic Energy Sciences (Contract DEFG0386ER-13608). We received considerable assistance from our colleagues Howard Littell, Curtis Nelson, and Debora Compton.

References

[1]Shizawa, T., and Eaton, J. K., "Mean Flow Development of a Longitudinal Vortex Embedded in an Attached, Three-Dimensional, Turbulent Boundary Layer," *International Symposium of Engineering Turbulence Modelling and Measurements*, Dubrovnik, Yugoslavia, 1990.

[2]Westphal, R. V., Pauley, W. R., and Eaton, J. K. "Interaction Between a Vortex and a Turbulent Boundary Layer, Part 1: Mean Flow Evolution and Turbulence Properties," NASA TM 88361, 1987.

[3]Arnaud, G. L., and Russell, D. A., "Symmetry-Plane Model for Turbulent Flows with Vortex Generators," AIAA-91-0723, 1991.

[4]Pauley, W. R., and Eaton, J. K., "The Fluid Dynamics and Heat Transfer Effects of Streamwise Vortices Embedded in a Turbulent Boundary Layer," Rept. MD-51, Mechanical Engineering Dept., Stanford Univ., Stanford, CA, 1988.

[5]Shizawa, T., and Eaton, J. K., "Interaction of an Embedded Longitudinal Vortex with an Attached, Three-Dimensional, Turbulent Boundary Layer," Rept. MD-56, Mechanical Engineering Dept., Stanford Univ., Stanford, CA, Aug. 1990.

[6]Shabaka, I. M. M. A., Mehta, R. D., and Bradshaw, P., "Longitudinal Vortices Imbedded in Turbulent Boundary Layers. Part 1. Single Vortex," *Journal of Fluid Mechanics* Vol. 155, 1985, pp. 37–57.

[7]Mehta, R. D., and Bradshaw, P., "Longitudinal Vortices Imbedded in Turbulent Boundary Layers. Part II. Vortex Pair with "Common Flow Upwards," *Journal of Fluid Mechanics*, Vol. 188, 1988, pp. 529–546.

[8]Takagi, S., and Sato, H., "An Experiment on the Interaction of a Turbulent Boundary Layer and a Row of Longitudinal Vortices," *Journal of the Japanese Society of Fluid Mechanics*, Vol. 2, 1983, pp. 288–300.

[9]Eibeck, P. A., and Eaton, J. K., "The Effects of Longitudinal Vortices Embedded in a Turbulent Boundary Layer on Momentum and Thermal Transport," *Proceedings of the 8th International Heat Transfer Conference*, 1986, pp. 1115–1120.

[10]Matsumoto, A., "Turbulent Boundary Layer Perturbed by Streamwise Vortices," *Journal of the Japan Society for Aeronautical and Space Sciences*, Vol. 34, 1986, pp. 141–152.

[11]Cutler, A. D., and Bradshaw, P., "The Interaction Between a Strong Longitudinal Vortex and a Turbulent Boundary Layer," AIAA-86-1071, 1986.

[12]Anderson, S. D., and Eaton, J. K., "Reynolds Stress Development in Pressure-Driven Three-Dimensional Turbulent Boundary Layers," *Journal of Fluid Mechanics*, Vol. 202, 1989, pp. 263–294.

[13]Bradshaw, P., and Pontikos, N. S. "Measurements in the Turbulent Boundary Layer on an 'Infinite' Swept Wing," *Journal of Fluid Mechanics*, Vol. 159, 1985, pp. 105–130.

[14]Bradshaw, P. "Effects of Streamline Curvature on Turbulent Flow," AGARDograph 169, 1973.